Measurements of few-mode fiber photonic lanterns in emulated atmospheric conditions for a low earth orbit space to ground optical communication receiver application

Sarah A. Tedder*[a], Bertram Floyd[b], Yousef K. Chahine[a,] Benjamin Croop[c], Brian E. Vyhnalek[a], Christopher Betters[d] and Sergio G. Leon-Saval[d]
[a]NASA Glenn Research Center, 21000 Brookpark Rd, Cleveland, OH, USA 44135-3127;
[b]Hx5 Sierra, 21000 Brookpark Rd, Cleveland, OH, USA 44135-3127;
[c]CREOL, University of Central Florida, 4303 Scorpius St, Orlando, FL, USA 32816-2700;
[d]Institute of Photonics and Optical Science, University of Sydney, NSW 2006, Sydney, Australia;

ABSTRACT

Photonic lanterns are being evaluated as a component of a scalable photon counting real-time optical ground receiver for space-to-ground photon-starved communication applications. The function of the lantern as a component of a receiver is to efficiently couple and deliver light from the atmospherically distorted focal spot formed behind a telescope to multiple small-core fiber-coupled single-element super-conducting nanowire detectors. This architecture solution is being compared to a multimode fiber coupled to a multi-element detector array. This paper presents a set of measurements that begins this comparison. This first set of measurements are a comparison of the throughput coupling loss at emulated atmospheric conditions for the case of a 60 cm diameter telescope receiving light from a low earth orbit satellite. The atmospheric conditions are numerically simulated at a range of turbulence levels using a beam propagation method and are physically emulated with a spatial light modulator. The results show that for the same number of output legs as the single-mode fiber lantern, the few-mode fiber lantern increases the power throughput up to 3.92 dB at the worst emulated atmospheric conditions tested of D/r_0=8.6. Furthermore, the coupling loss of the few-mode fiber lantern approaches the capability of a 30 micron graded index multimode fiber chosen for coupling to a 16 element detector array.

Keywords: Photonic lanterns, fiber coupling, free-space optical communications, photon counting, and ground receiver.

1. INTRODUCTION

Standardized, commercial off-the-shelf component based, as well as scalable space-to-ground optical receiver solutions are needed to increase the affordability and availability of ground stations for a wide range of public or private photon counting applications. NASA Glenn Research Center is developing a ground receiver that includes the aft optics, detector, and real time FPGA-based receiver[1]. Our goals are to develop a receiver architecture that is scalable in terms of: data rate, atmospheric conditions, and telescope designs, while using commercial components whenever possible and implementing the Consultative Committee for Space Data Systems Optical Communications High Photon Efficiency standard[2].

This paper focuses on the component that efficiently delivers light from an atmospherically distorted focal spot formed behind a telescope to commercially available single photon super-conducting nanowire detectors that are butt-coupled to fibers. Two fiber solutions are being evaluated: a photonic lantern and a multimode fiber. These solutions would require different detector designs. For the photonic lantern solution, the light would be coupled to multiple small-core fiber-coupled single-pixel nanowire elements. Alternatively, the multimode fiber would couple to a multi-element array of nanowire detectors on a single chip. Here we consider the following specific designs: for the photonic lanterns - seven output legs to be coupled to seven 14 micron diameter detectors; and for the multimode fiber– a 30 micron diameter graded index core to be coupled to a 16 multi-element single chip array.

Although the laser output from a spacecraft has a Gaussian profile, light arriving and coupling to the telescope is multi-moded in nature due to atmospheric turbulence that distorts the beam profile by scattering energy and phase into higher-order modes. Therefore, a multimode fiber capable of supporting enough higher-order spatial modes to account for the distorted atmospheric wavefront must be used in order to couple light efficiently from a telescope to an optical waveguide.

*sarah.a.tedder@nasa.gov; phone 1 216 433-6591; nasa.gov

Photonic lanterns were initially invented to increase the coupling efficiency of light collected aft of telescopes and deliver it to multiple single-mode fiber Bragg gratings for astronomical applications[3]. Since then, their use for optical communication and light detection and ranging (LIDAR) receivers has been explored by others[4-9].

Standard photonic lanterns fabricated from single-mode fibers (SMF) have a ratio of one fiber spatial mode to one fiber output leg in order to conserve entropy and give a low-loss transition device. Therefore, guidance of higher order modes of a lantern is dependent on the number of output legs. For the receiver design under consideration[1], the number of detectors increases with the number of lantern output legs, raising the overall cost and complexity of the system. Depending on the condition and desired data rate, the number of detectors needed for efficient coupling could be higher than the number of detectors required to compensate for dead time. Hence, a lantern fabricated with few-mode fibers (FMF) was proposed and introduced in previous work[10] to break the dependence of increased mode coupling capacity with number of output fiber legs, thereby reducing the overall number of detectors. Previously, we presented measurements of the first lantern fabricated completely with FMFs, demonstrating that it has a larger coupling efficiency at higher order fiber spatial modes than a lantern fabricated with SMFs with a matching number of output legs[10].

This paper begins a comparison study of the two fiber/detector solutions under consideration by measuring total coupling loss at emulated atmospheric conditions of a 60 cm diameter telescope from a low earth orbit emitter. The atmospheric conditions were numerically simulated with a beam propagation model. These simulations were then used to generate complex amplitude phase holograms, which were applied to a laser beam with spatial light modulator to emulate a laser beam affected by the atmosphere. While the simulations have been verified in section 2.2, the emulations accuracy has yet to be fully characterized (see section 2.3); thus the measurements presented in this paper should be considered preliminary.

The first measurements presented in this paper are the coupling loss of fiber and lanterns at a range of numerical apertures (NAs). These measurements enable the determination of the best optical design for maximum coupling efficiency. Next, the throughput coupling efficiency of a 7:1 FMF lantern is compared to a 30 micron graded-index multimode fiber (GI-MMF) and a 7:1 SMF lantern at a range of turbulence levels. The focus of this paper is to compare power throughput of the fiber components and does not include an evaluation of the fiber to detector coupling. For information on the coupling of the FMFs to the single element super-conducting nanowire detectors, please see the article by Vyhnalek et al[11].

2. EXPERIMENTAL SETUP

The coupling losses presented in this paper were measured using the optical setup shown in Figure 1. First, a linearly polarized fiber-coupled 1550 nm laser is used as the light source. The light exiting the polarized SMF is collimated with a 50.8 mm focal length reflective collimator (RC) to a 7.00 mm diameter beam. The linear polarization direction of the light was then aligned to the spatial light modulator's (SLM) polarization sensitivity axis with a half-wave plate (HWP). The light is then passed through a 50/50 beam splitter (BS) with half of the light reaching the SLM's 12.8 mm × 12.8 mm surface comprised of an array of 512 x 512 active liquid crystal pixels. Next, the SLM reflects the light back to the 50/50 beam splitter sending half of that energy into a 40 mm focusing lens (L1). The light then passes through a 200 micron pinhole (PH) to select only the first order reflection from the SLM. The light is then collimated with a 40 mm lens (L2) back to a 7.00 mm diameter beam. When needed, a mirror (M1) is placed between L2 and L3 to inspect the beam with a beam profiler camera. A focusing lens (L3) is then used to focus the light into the lantern or fiber under test. To test a range of effective NAs of the input light, lenses with a range of focal lengths were used as L3. The range of focal lengths used are shown in Table 1. These focal lengths were used with a 7.00 mm beam to produce the corresponding effective NAs listed in Table 1.

Table 1: Focal lengths of lenses used to produce the corresponding effective numerical apertures.

Focal length, mm	18	20	25	32	40	50	60	79
Numerical Aperture	0.194	0.175	0.14	0.109	0.0875	0.07	0.0583	0.0443

The test fiber or lantern is placed at the focal point of the focusing lens with a three dimensional fine positioner. To determine the efficiency, the input power is measured with a power meter (PM1) having a 9.7 mm × 9.7 mm active surface just after the focusing lens. The output power is measured with an 8 channel power meter (PM2) at the exit of the fiber or lantern. The coupling loss was determined by taking the difference between the input and output powers; therefore, our

coupling loss values presented in the results included the internal losses of the photonic lantern transition. Control of the SLM and power meters was automated to allow the testing of 100 inputs on the SLM.

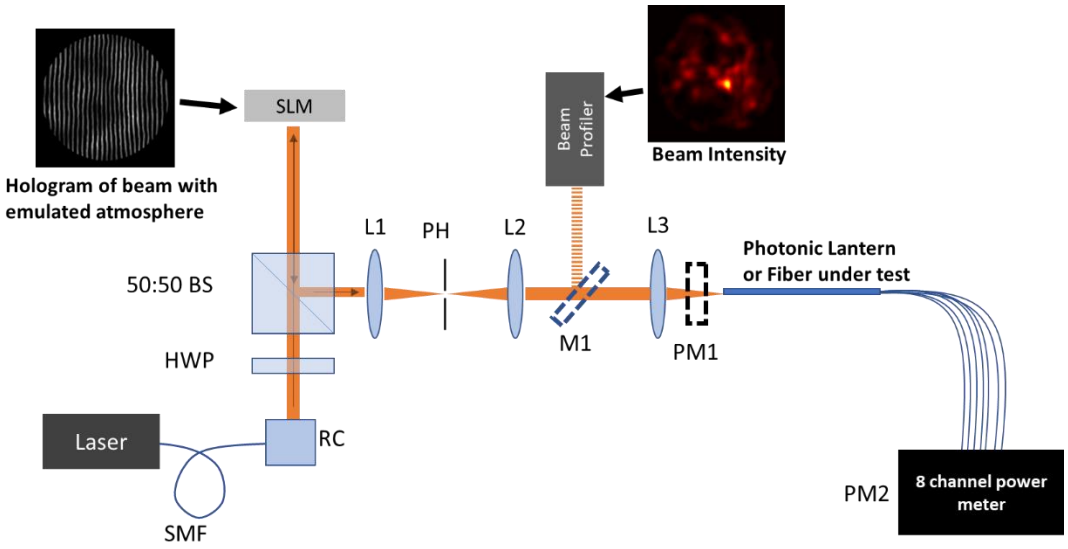

Figure 1: Schematic of the experimental setup for measuring the coupling efficiency of each device (not to scale)

2.1 Photonic Lanterns and Fibers

Two types of photonic lanterns were fabricated at the NASA Glenn Research Center with a commercial fiber processing machine: one made with SMFs and one made with FMFs. For this application, the light is coupled into the MMF side of the lantern and split to 7 SMFs or FMFs that are butt-coupled on the detectors. The physical dimensions of these lanterns and the SMFs and FMFs they are fabricated with are summarized in Table 2. Table 2 also includes the specifications of the 30 micron GI-MMF that was measured to compare throughput performance for the alternate detector solution.

The 7:1 SMF lantern was designed to have a 30 micron core with an input NA of 0.09. The lantern transition from the MMF input to the 7 SMFs was a 40 mm long taper. The 7:1 SMF lantern was made using 7 SMF that had NAs of 0.11-0.13 at 1550 nm. The SMF lantern can couple the first 7 fiber spatial modes: LP_{01}, LP_{11a}, LP_{11b}, LP_{21a}, LP_{21b}, LP_{02}, and LP_{31a}[12]. The FMF lantern is made with 7 graded index FMFs that each allow 6 spatial modes, LP_{01}, LP_{11a}, LP_{11b}, LP_{21a}, LP_{21b}, and LP_{02}. The transition length from the 55 micron diameter and NA of 0.126 multimode core end of the lantern to the FMFs independent cores is 70 mm. As we use the photonic lantern as collecting light buckets from the multimode to the few-mode end, in order to minimize losses in the system, the number of modes supported by the output legs should be slightly more than the number supported by the multimode side of the lantern[4]. The 7:1 FMF lantern fabricated has 41 modes while the 7 output fibers should have a collective number of 42 modes at our operating wavelength of 1550 nm.

Table 2: Photonic Lanterns and Fiber Tested

Fiber	Input Core Size, µm	Input Numerical Aperture	# of modes supported (counting spatial degeneracies)
Single-Mode Fiber	9[a]	0.12	1
Graded Index Few-Mode Fiber	20	0.19	6
Graded Index Multi-Mode Fiber	30	0.2	15
7:1 SMF lantern	30	0.09	7
7:1 FMF lantern	55	0.126	41[b]

[a]Mode Field Diameter. [b]Number of modes supported by the MMF side of the lantern.

2.2 Simulation of the atmospheric disturbed wavefront

The simulation of the atmospheric turbulence was verified with theory before being used to test the performance of the fibers and lanterns. The atmospherically disturbed wavefront was numerically simulated using the split-step beam propagation algorithm modeling an atmospheric channel from a space-based transmitter to a ground receiver. The atmospheric propagation path is split into 5 thick slabs and the turbulence-induced distortion of the beam in each slab is represented by a randomly generated two-dimensional phase screen modeling the effect of propagation through Kolmogorov turbulence in the corresponding slab. For this work, we have assumed the refractive index structure constant characterizing the strength of the turbulence depends on altitude according to the Hufnagel-Valley profile. The effective structure constant for each phase screen is then determined by integration over the corresponding propagation segment.

For a transmitter in low earth orbit, the distorted optical field at the aperture of a ground-based telescope is effectively that of a plane wave after propagation through the atmosphere making it unnecessary to specify the beam precisely at the transmitter. For this work, we thus model a plane wave propagating along a 24 km vertical atmospheric path (i.e. vacuum propagation is assumed above 24 km) incident upon a 60 cm diameter collection aperture (D) with atmospheric coherence lengths (r_0) of 7 cm, 15 cm, 30 cm, and 50 cm. In terms of the imaging parameter (D/r_0), results were obtained at the corresponding D/r_0 values of 8.6, 4, 2, and 1.2. For each test a baseline measurement was made with an unperturbed beam profile ($D/r_0 = 0$); i.e. a flat top profile. This uniform intensity flat top beam was also used to align to the fiber or lantern at the focus of a converging lens. This alignment was maintained for the measurements involving the distorted beam profiles ($D/r_0 > 0$).

For each turbulence level, 100 beam profiles were numerically simulated and the atmospheric coherence length r_0 of the simulated optical fields at the collection plane (for input to fiber device) was verified by examination of the wave structure function (see e.g. Fried[13] for the definition).

The atmospheric coherence length r_0 introduced by Fried[13] is defined in terms of the wave structure function under the assumption that for a plane wave in locally homogeneous and isotropic turbulence, the wave structure function depends only on the separation distance $r = |\vec{r}|$ between two field points and has the form

$$D(r) = 6.88\left(\frac{r}{r_0}\right)^{5/3}. \tag{1}$$

Moreover, based on the Rytov theory the atmospheric coherence length r_0 can be given in terms of the structure parameter C_n^2(z) along the propagation path $z = 0$ to $z = L$ via[14]

$$r_0 = \left(0.423k^2 \int_0^L C_n^2(z)dz\right)^{-3/5}. \tag{2}$$

To verify the simulations, the wave structure functions for the fields generated at each turbulence level were computed and plotted in Figure 2 against the theoretically predicted wave structure function based on the continuous C_n^2 profile (Equations 1 and 2). First, the 5/3-law behavior expected from Equation 2 is verified in the region of interest, and thus the simulated atmospheric coherence length can be validated by comparison with the theoretical curves in Equation 1. The wave structure function computed from the simulated data (shown in symbols) matches with the theory (shown with lines) as expected in the mid-separation distance region. The disagreement at larger separations is a well-documented limitation of the phase screen-based split-step method[15]. For further details concerning the method, the atmospheric model, and the validation of the numerical beam propagation code, see Chahine et al[16].

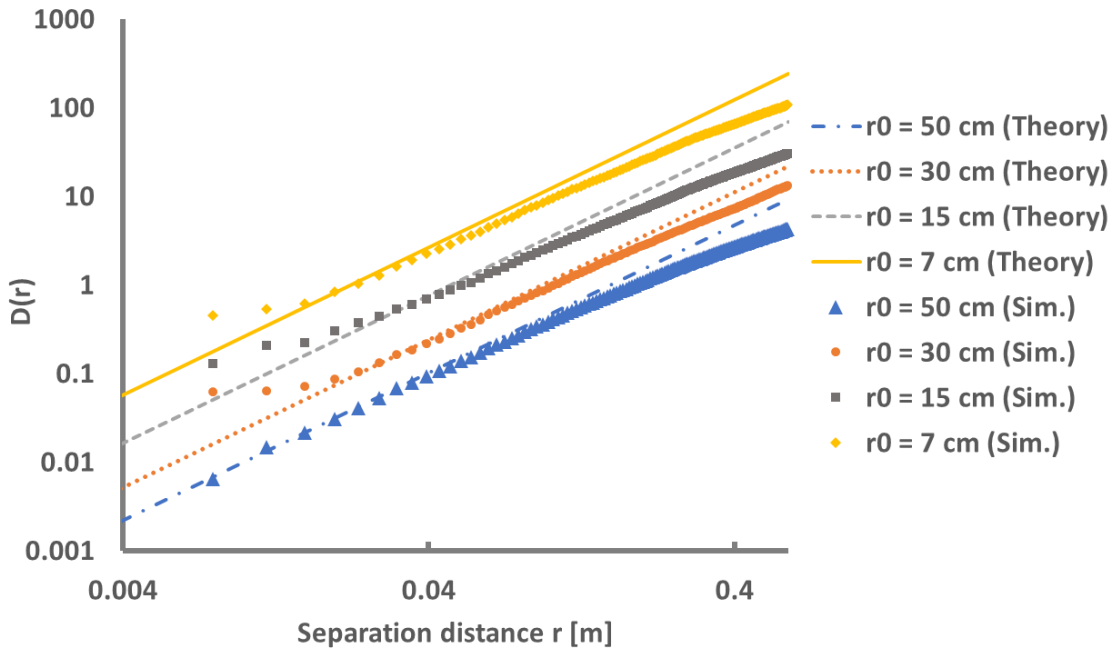

Figure 2: Comparison of simulation for r_0 = 7, 15, 30, and 50 cm to theory of the wave structure function versus separation distance. Theoretical results are plotted as lines, and simulated results are plotted as symbols.

2.3 Emulation of the atmospheric disturbed wavefront

The SLM was used to emulate 100 resulting wavefronts from the simulation. The wavefronts were created by encoding complex amplitude phase holograms of the simulated beam output on the SLM[17]. When a hologram is applied to the SLM, the phase and amplitude of the Gaussian beam is modified to create the desired wavefront. Figure 3 a) shows the hologram created from the simulated wavefront shown in b) with r_0 of 50 cm, which was applied to achieve the intensity profile pictured in c). The created intensity profile has similar features to the simulated profile but the features appear to be less resolved. Measurements of the modulated profile with a beam profiler camera were collected and analyzed to determine if the created r_0 matched the input r_0 based on intensity statistics, but the results were inconclusive because the intensity is an indirect measurement of the phase characteristic, r_0. Measurements of the phase front will conclusively assess the accuracy of r_0. Therefore, although the simulation has been fully verified, the emulation has not. Further emulation work will be conducted in future studies.

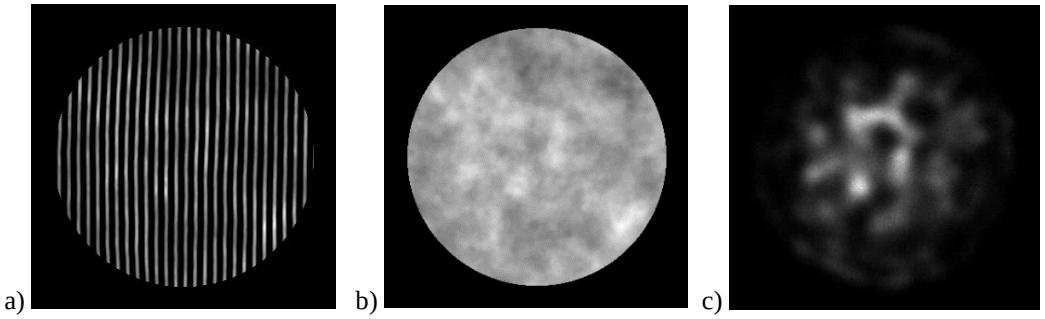

Figure 3: A sample of wavefront creation at r_0 = 50 cm. (a) phase hologram, (b) simulated intensity profile, (c) created intensity profile. Note the color scales in (b) and (c) are not the same.

3. RESULTS AND DISCUSSION

This section presents the coupling loss of a 7:1 FMF lantern, a 7:1 SMF lantern, and 30 micron GI-MMF for a range of input NAs as displayed in Table 1 and emulated D/r_0 values (0, 1.2, 2, 4, and 8.6) for a 60 cm diameter telescope receiving light from low earth orbit. The coupling loss presented is the power throughput of the fiber and lanterns and does not include coupling to the detectors. Furthermore, coupling losses here represent input coupling losses in the case of the multimode fiber; and input coupling losses plus transition losses in the photonic lantern cases.

3.1 Evaluation of the minimum coupling loss of free space light for different input numerical apertures

To evaluate the best NA that minimizes the free space light coupling loss to the lanterns and fibers in our optical system, the devices were measured over a range of NAs at each D/r_0. Sample results for the FMF lantern are shown in Figure 4, which plots the coupling loss of the FMF lantern versus the input NA at three different D/r_0 values. The symbols indicate the average loss from 100 atmospheric emulations and the error bars indicate the standard deviation from the mean. The plot shows the FMF lantern's minimum input coupling loss occurs at different NAs for different D/r_0. At the highest turbulence level, D/r_0 of 8.6 (shown in purple diamonds), the lantern's minimum coupling loss occurs at 0.109. This is near the lantern's design NA of 0.126. While at D/r_0 of 1.2 (red crosses), the lowest turbulence level, the minimum coupling loss occurs at an NA of 0.06.

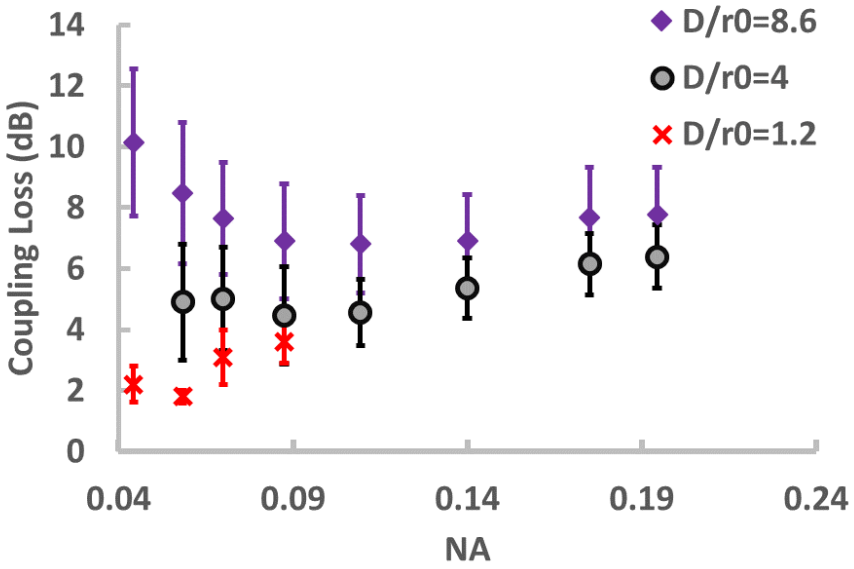

Figure 4: Coupling loss of the 7:1 FMF lantern at a range of NAs for 3 sample D/r_0.

To further evaluate this behavior, Figure 5 compares the best input coupling NAs at each D/r_0 value tested for all of the devices. The figure shows results for the FMF photonic lantern in blue squares, the SMF lantern in green triangles, and the GI-MMF in orange circles. The symbols are the NA at which the minimum loss was collected and the error bars represent resolution of the tested NA. The resolution is defined to be the midpoint between the tested NA and the next closest NA that could be tested. Note: D/r_0 of zero indicates an unperturbed top-hat propagated beam.

The best input coupling NA of the GI-MMF is constant across the tested D/r_0 values. In contrast, the SMF and FMF lanterns both show a dependence of the best input coupling NA on the D/r_0 value in our optical setup. Both lanterns show the general trend that the best NA for minimum coupling losses increases with increasing D/r_0. Increasing D/r_0 values corresponds to increased turbulence levels at which more energy is scattered to higher spatial modes. Therefore, Figure 5 indicates as the energy of the beam is scattered to higher order spatial modes, larger NAs are required to optimize the overlap of the free space spatial modes to the modes supported by the lanterns. Further study is required to understand the source of this trend.

The variances of the best performing input coupling NAs for the lanterns indicate that a fixed focal length optical design could cause up to 2 dB of losses over the range of tested D/r_0 values. However, the range tested here is likely to be larger

than an operational range that would be experienced. For example, the operational range measured in Giggenbach et al[18] was r_0 ~10 cm to 20 cm making the D/r_0 range only from 3 to 6. Since D/r_0 of 3 and 6 were not measured, we cannot quantify the maximum loss that would be experienced for this example. But if another reduced range of D/r_0 4 to 8.6 was considered, and the input optics were designed for D/r_0 of 8.6, then the largest loss would be 0.09 dB.

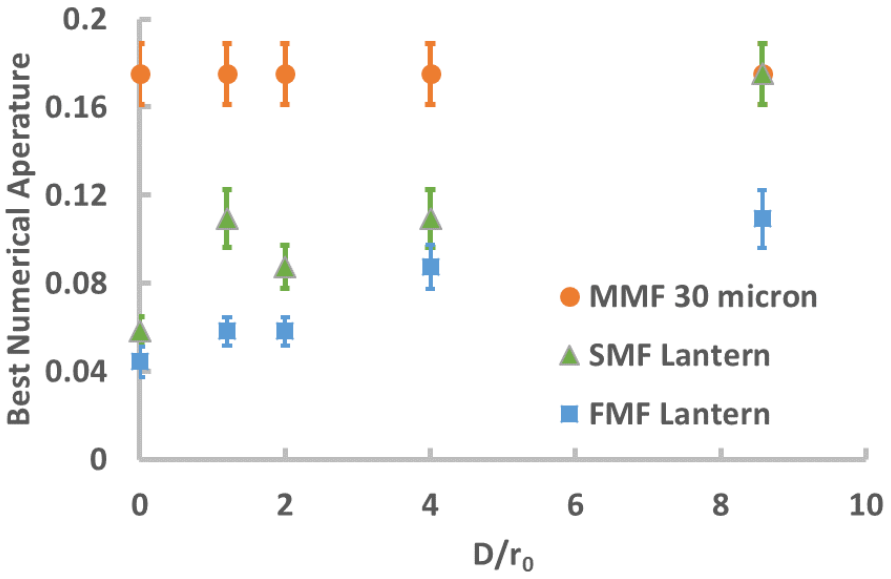

Figure 5: Best input coupling numerical aperture for minimum input coupling loss versus D/r_0 for the GI-MMF, SMF lantern and FMF lantern.

3.2 Minimum input coupling loss for all devices over a range of D/r_0

To compare the input coupling loss of the devices to each other over the range of tested D/r_0, the minimum input coupling loss at the best performing input NA (for each respective device) is plotted in Figure 6. The symbols show the average coupling loss for 100 random atmospheric perturbations at each D/r_0, while the error bars indicate the standard deviation. The GI-MMF has the lowest coupling loss at all conditions, followed by the FMF lantern. The SMF lantern has the highest coupling loss, as anticipated by the lower number of waveguide modes that couple to the system.

Table 3 presents the same results given in terms of difference in input coupling loss relative to the FMF lantern. The FMF lantern shows gains of 1 to 4 dB over the SMF lantern. This indicates the coupling efficiency of the FMF lantern was increased by increasing the number of modes available per fiber leg over the SMF lantern. As the energy of the modes is spread to higher order modes (increasing D/r_0) the difference in coupling efficiency between the SMF lantern and FMF lantern further increases.

The FMF lantern approaches, but does not reach, the same input coupling loss performance as the GI-MMF with differences between 0.53 and 1.83 dB. This is despite the fact that the design of FMF lantern predicts 41 spatial modes while the GI-MMF only has 15. However, the input coupling loss of the FMF lantern also includes the transition losses of the device. Further studies of the optimal FMF lantern design, and theoretical mode transition behavior, are needed to reduce or explain the difference in performance from the GI-MMF.

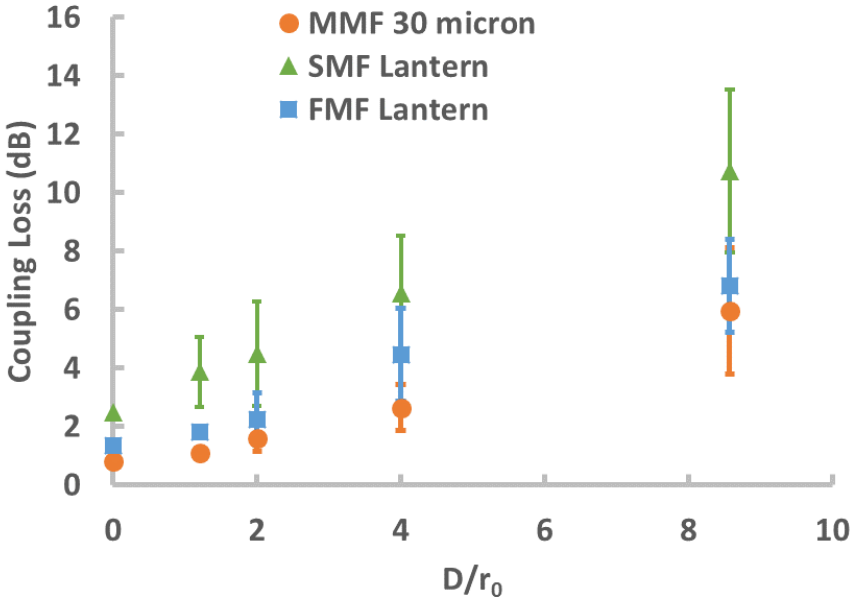

Figure 6: Plot of the input coupling loss at their best performing input coupling NA verses the D/r_0 for the 30 micron GI-MMF, SMF lantern, and FMF lantern.

Table 3: FMF lantern coupling loss compared to a SMF lantern and the 30 micron GI-MMF

D/r_0	Gain Relative to the SMF Lantern (dB)	Loss Relative to the GI-MMF (dB)
8.6	3.92	0.86
4.0	2.10	1.83
2.0	2.25	0.66
1.2	2.07	0.69
0 (unperturbed)	1.17	0.53

4. CONCLUSION

In conclusion, a preliminary case study of a 60 cm diameter telescope receiving light from telescope was performed to compare two fiber device solutions for a real-time optical ground receiver. The effect of the input NA and turbulence level of the emulated atmospheric conditions were measured for two types of lanterns and a GI-MMF.

Both lantern types tested show a different relationship between the coupling losses and input NA than GI-MMFs. While the best input NA of the GI-MMF is independent of the atmospheric condition, the lanterns show a dependence. We conjecture, that this dependence may be imposed by the change of the focused spot size with the varying NAs and its effect on the overall overlap and coupling to the photonic lantern modes. This overall behavior indicates that a fixed optical design may cause non-optimal coupling performance for lanterns if we consider a very large operational range of D/r_0. But if the lanterns are used in a limited operational range then the effect can be as small as ~0.1 dB. Therefore, the coupling optics for the lantern should be designed for the operational range. The reason for the latnerns' dependence of optimal NA on turbulence level is not yet understood and will be explored and studied in future work.

At best NAs the results presented show that FMF lanterns have increased coupling efficiency over SMF lanterns at the emulated turbulence levels tested. At these same conditions, the FMF lanterns have slightly more throughput coupling loss than a 30 micron GI-MMF. This indicates that a FMF lanterns with slight improvements may be a possible solution for the scalable ground receiver under development.

Much more work is needed to compare the FMF lantern and GI-MMF solutions. First, an important factor of the FMF lantern not explored in this paper is the how much the splitting of the light to the output legs contributes to detector blocking loss caused by dead time[19]. The splitting of the FMF lantern was compared to SMF lanterns in previous work[10]. The effect of emulated atmosphere on the detector blocking loss contributed by the FMF lantern needs to be compared to the GI-MMF coupling efficiency to the 16 element detector array.

Second, this study was performed by emulating the atmosphere with a SLM. While the simulation used to create the emulation was verified, the indirect method of evaluating the emulation accuracy produced inconclusive results. Therefore, in future work a direct assessment of the emulation accuracy will be performed using a wavefront sensor.

Third, the design and fabrication of the FMF lantern will be studied in an effort to understand and reduce its input coupling and transition losses. Design factors include the effects of varying the core diameter and transition taper length. Theoretical modeling of the modes of the lanterns will be performed as well as their overlap with realistic atmospheric turbulence situations. Measurement of the coupling loss of the FMF lanterns with its own theoretical modes will be performed. This will enable further understanding of its operational behavior. Further, measurements will be made at more emulated atmospheric conditions with a focus on typical operational values for ground stations. Finally, a system-level comparison of the two system options will be compared by measuring the coupling loss of the GI-MMF to the 16 element detector array and comparing the combined losses.

ACKNOWLEDGEMENTS

This work is supported by the NASA Space Communications and Navigation (SCaN) Program and the Glenn Research Center Communications & Intelligent Systems Division. This work was also supported by the Sydney Astrophotonic Instrumentation Laboratory (SAIL) at the University of Sydney.

REFERENCES

[1] Vyhnalek, B., Nappier, J., Tedder, S., “Real Time Photon-Counting Receiver for High Photon Efficiency Optical Communications”, IEEE ICSOS, (2019).

[2] “Optical Communications Coding and Synchronization Draft Recommended Standard,” CCSDS 142.0-R-1 Blue Book (2019).

[3] Birks, T., Gris-Sanchez, I., Yerolatisitis, S., Leon-Saval, S. G., and Thompson, R. R., “The photonic lantern”, Advances in Optics and Photonics, (7) (2015).

[4] Ozdur, I., Toliver, P., Agarwal, A., and Woodward, T. K., “Free-space to single-mode collection efficiency enhancement using photonic lanterns”, Optics Letters, Vol. 38 (18) (2013).

[5] Yarnall, T., Geisler, D., Schieler, C., and Yip, R., “Analysis of Free-Space Coupling to Photonic Lanterns in the Presence of Tilt Errors”, IEEE Photonics Conference, 17393311, (2017).

[6] Geisler, D., Yarnall, T., Scheiler, C., Lund, G., Stevens, M., Robinson, B., Hamilton, S., “Ground Receiver Architectures Enabled by Digital Coherent Combing”, Advanced Photonics Congress, OSA, (2018).

[7] Geisler, D., Yarnall, T., Lund, G., Schieler, C., Stevens, M., Fontaine, N., Robinson, B., and Hamilton, S., “Experimental comparison of 3-mode and single mode coupling over a 1.6-km free-space link”, Proc. SPIE Free-Space Laser Communication and Atmospheric Propagation XXX; 105240H (2018).

[8] Sergio G. Leon-Saval, Christopher H. Betters, Joel R. Salazar-Gil, Seong-Sik Min, Itandehui Gris-Sanchez, Tim A. Birks, Jon Lawrence, Roger Haynes, Dionne Haynes, Martin Roth, Sylvain Veilleux, and Joss Bland-Hawthorn, "Divide and conquer: an efficient solution to highly multimoded photonic lanterns from multicore fibres," Opt. Express **25**, 17530-17540 (2017)

[9] Ozdur, I., Toliver, P., and Woodward, T. K., “Photonic-lantern-based coherent LIDAR system”, Optics Express, Vol. 23 (4) (2015).

[10] Tedder, S., Vyhnalek, B., Leon-Saval, S., Betters, C., Floyd, B., Staffa, J., and Lafon, R., "Single-mode fiber and few-mode photonic lanterns performance evaluated for use in a scalable real-time photon counting ground receiver", Proc. SPIE Free-Space Laser Communication and Atmospheric Propagation XXXI, 109100G (2019).
[11] Vyhnalek, B., Tedder, S., Katz, E, and Nappier, J. "Few-mode fiber coupled superconducting nanowire single-photon detectors for photon efficient optical communications," Proc. SPIE Free-Space Laser Communication and Atmospheric Propagation XXXI 10910 (11) (2019).
[12] Leon-Saval, S., Argyros, A., and Bland-Hawthorn, J., "Photonic lanterns: a study of light propagation in multimode to single-mode convertors", Optics Express, Vol. 18 (8) (2010).
[13] Fried, D. L., "Optical resolution through a randomly inhomogeneous medium for very long and very short exposures", Journal of the Optical Society of America, Vol. 56 (10) (1966).
[14] Hufnagel, R. E., Stanley, N. R., "Modulation transfer function associated with image transmission through turbulent media", Journal of the Optical Society of America, Vol. 54 (1) (1964).
[15] Schmidt, J., [Numerical simulation of optical wave propagation with example in MATLAB], SPIE, Bellingham, Washington, 167-182, (2010).
[16] Chahine, Y., Tedder, S., and Vyhnalek, B., "Beam propagation through atmospheric turbulence using an altitude-dependent structure profile with non-uniformly distributed phase screens", Proc. SPIE, Free-Space Laser Communication and Atmospheric Propagation, XXXII (2020).
[17] Rosales-Guzman, C. and Forbes, A., [How to Shape Light with Spatial Light Modulators], SPIE Press, Bellingham, Washington, 14-17 (2017).
[18] Giggenbach, D., Becker, P., Ramon, M., Fuchs, C., Sodnik, Z., and Zayer, I., "Lunar Optical Communications Link (LOCL) Measurements of Received Power Fluctuations Wavefront Quality," Proc. International Conference on Space Optical Systems and Applications (ICSOS), Japan, May 7-9 (2014).
[19] Moison, B. and Piazzolla, S., "Blocking losses on an optical communications link", Proc. IEEE International Conference on Space Optical System and Applications, (2011).